Inorg. Chem. **2005**, *44*, 6725–6735

Cyclic $M_2(RL)_2$ Coordination Complexes of 5-(3-[*N*-*tert*-Butyl-*N*-aminoxyl]phenyl)pyrimidine with Paramagnetic Transition Metal Dications

Martha Baskett,[†] Paul M. Lahti,*[,†] Armando Paduan-Filho,[†,‡] and Nei F. Oliveira, Jr.[‡]

Department of Chemistry, University of Massachusetts, Amherst, Massachusetts 01003, and Instituto de Fisica, Universidade de São Paulo, S. P., Brazil

Received March 23, 2005

5-(3-(*N*-*tert*-Butyl-*N*-aminoxyl)phenyl)pyrimidine (RL = 3NITPhPyrim) forms isostructural cyclic $M_2(RL)_2$ cyclic dimers with $M(hfac)_2$ (M = Mn, Co, Cu; hfac = hexafluoroacetylacetonate). $Mn_2(hfac)_4(RL)_2$ exhibits strong antiferromagnetic Mn–RL exchange, with weak ferromagnetic exchange (0.7 cm^{-1}) between Mn–RL units that is consistent with a spin polarization exchange mechanism. The magnetic moment of $Co_2(hfac)_4(RL)_2$ at higher temperatures is consistent with strongly antiferromagnetic exchange within the Co–NIT units and tends toward zero below 50 K at lower magnetic fields. $Cu_2(hfac)_4(RL)_2$ shows more complex behavior, with no high-temperature plateau in $\chi T(T)$ up to 300 K but a monotonic decrease down to about 100 K. The Cu(II)–nitroxide bonds decrease by 0.2–0.3 Å over the same temperature range, corresponding to a change of nitroxide coordination from axial to equatorial. This thermally reversible Jahn–Teller distortion leads to a thermally induced spin state conversion from a high-spin, paramagnetic state at higher temperature to a low-spin state at lower temperature. This spin state conversion is accompanied by a reversible solid-state thermochromic change between dull yellow-brown at room temperature and green at 77 K.

Introduction

The synthesis of coordination complexes between paramagnetic cations and organic radical-ligands is a fruitful field of study that has provided much information about structure−property relationships for intramolecular exchange interactions and molecular magnetism.[1] Modest changes in the structure of radical-ligands or in the coordination sphere of such complexes can sometimes lead to large changes in electronic behavior. As a result, a substantial amount of effort in this area is ongoing, much of it aimed to identify predictive structure−property trends.

Although a number of paramagnetic systems have been reported with a general $M_2(L)_2$ dimer structure,[1,2] we restrict our attention to cyclic $M_2(RL)_2$ complexes where RL = radical-ligand; hence, the organic fragment and the metal ion bear unpaired spins. A variety of examples have been reported where the RL spin-bearing unit is nitronyl nitroxide,[1a−c,f,h] iminoyl nitroxide,[1m−n] verdazyl,[1l−m] or aryl nitroxide.[1c−f,h,j] We have been most interested in systems incorporating R = aryl nitroxide, since these radical-ligands exhibit the following desirable features for molecular mag-

* To whom correspondence should be addressed. E-mail: lahti@chem.umass.edu.

† University of Massachusetts.

‡ Universidade de São Paulo.

(1) (a) Caneschi, A.; Gatteschi, D.; Sessoli, R.; Rey, P. *Acc. Chem. Res.* **1989**, *22*, 392. (b) Caneschi, A.; Gatteschi, D.; Sessoli, R. In *Magnetic Molecular Materials*; Gatteschi, D., Kahn, O., Miller, J. S., Palacio, F., Eds.; Kluwer: Dordrecht, The Netherlands, 1991; p 215. (c) Gatteschi, D.; Rey, P. In *Magnetic Properties of Organic Materials*; Lahti, P. M., Ed.; Marcel Dekker: New York, 1999. (d) Iwamura, H.; Inoue, K.; Hayamizu, T. *Pure Appl. Chem.* **1996**, *68*, 243. (e) Iwamura, H.; Inoue, K.; Koga, N.; Hayamizu, T. *NATO ASI Series, Series C: Mathematical and Physical Sciences*; Kluwer: Dordrecht, The Netherlands, 1996; Vol. 484, p 157. (f) Inoue, K.; Iwahori, F.; Markosyan, A. S.; Iwamura, H. *Coord. Chem. Rev.* **2000**, *198*, 219. (g) Miller, J. S.; Epstein, A. J. *MRS Bull.* **2000**, *25*, 21. (h) Veciana, J.; Iwamura, H. *MRS Bull.* **2000**, *25*, 41. (i) Itoh, K.; Kinoshita, M., Eds., *Molecular Magnetism: New Magnetic Materials*; Gordon and Breach: Newark, NJ, 2000. (j) Kahn, O. *Molecular Magnetism*; VCH: New York, 1993. (k) Ouahab, L. *Coord. Chem. Rev.* **1998**, *178−180*, 1501. (l) Hicks, R. G. *Aust. J. Chem.* **2001**, *54*, 597. (m) Lemaire, M., T. *Pure Appl. Chem.* **2004**, *76*, 277.

(2) Other M_2L_2 systems where L incorporates a radical include (not exclusively): (a) Ishimura, Y.; Inoue, K.; Koga, N.; Iwamura, H. *Chem. Lett.* **1994**, 1693. (b) Kitano, M.; Ishimaru, Y.; Inoue, K.; Koga, N.; Iwamura, H. *Inorg. Chem.* **1994**, *33*, 6012. (c) Ishimaru, Y.; Makoto Kitano, M.; Kumada, H.; Koga, N.; Iwamura, H. *Inorg. Chem.* **1998**, *37*, 2273. (d) Iwamura, H.; Koga, N. *Mol. Cryst. Liq. Cryst.* **1999**, *334*, 437. (e) Rabu, P.; Drillon, M.; Iwamura, H.; Gorlitz, G.; Itoh, T.; Matsuda, K.; Koga, N.; Inoue, K. *Eur. J. Inorg. Chem.* **2000**, 211. (f) Wang, H.; Liu, Z.; Liu, C.; Zhang, D.; Lu, Z.; Geng, H.; Shuai, Z.; Zhu, D. *Inorg. Chem.* **2004**, *43*, 4091.

10.1021/ic050435t CCC: $30.25
Published on Web 08/05/2005

netic design: (1) they have high stability, (2) they possess more delocalized unpaired spin distributions than nitronyl nitroxides or iminoyl nitroxides, allowing more possibilities for making structural connections with significant exchange interactions.

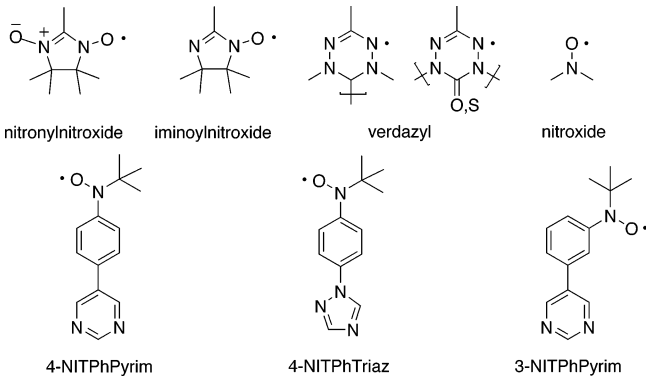

We have previously reported the synthesis and magnetic properties of $M_2(hfac)_4(RL)_2$ type complexes, where RL = 5-(4-(*N-tert*-butyl-*N*-aminoxyl)phenyl)pyrimidine[3a−b] and 1-(4-*(N-tert*-butyl-*N*-aminoxylphenyl))-1*H*-1,2,4-triazole[3c] (RL = 4NITPhPyrim and 4NITPhTriaz), and investigated their differences in behavior due to variation of M^{2+} and incorporation of π-alternant vs π-nonalternant ligands. As part of studies aimed at investigating differences in exchange behavior due to changing connectivity, we now report the synthesis, crystallography, and magnetic properties of the $M_2(hfac)_4(RL)_2$ complexes **1**−**3** of 5-(3-(*N-tert*-butyl-*N*-aminoxyl)phenyl)pyrimidine (3NITPhPyrim) with $M(hfac)_2$ (M = Mn, Co, Cu; hfac = hexafluoroacetylacetonate).

Methodology and Results

The synthesis of 3NITPhPyrim is shown in Scheme 1. Protected hydroxylamine **4** was made by a previously reported route[4] and then metalated and converted to the boronic acid **5**. While **5** and other boronic acids can form cyclic boroxins (not shown), either form is useful for carbon−carbon bond formation. Compound **5** was subjected to Pd-catalyzed coupling with 5-bromopyrimidine to give **6**, deprotected to precursor **7**, and oxidized using Ag_2O to the desired nitroxide. The solution phase electron spin resonance (ESR) spectrum of 3NITPhPyrim showed a nitroxide 1:1:1 triplet with a_N = 12.3 G and additional hyperfine coupling (hfc) from the phenyl protons but no resolvable hfc from the pyrimidine ring. The *meta*-connectivity of 3NITPhPyrim disallows direct conjugation of the nitroxide spin onto the pyrimidine ring. UB3LYP/EPR-II computations[5,6] show that the ligating nitrogen atoms in 3NITPhPyrim have Mulliken spin populations of only ∼0.1%.

Although **7** was readily isolated with acceptable elemental purity, 3NITPhPyrim itself was a somewhat unstable red oil

Scheme 1. Synthesis of Complexes **1**−**3**

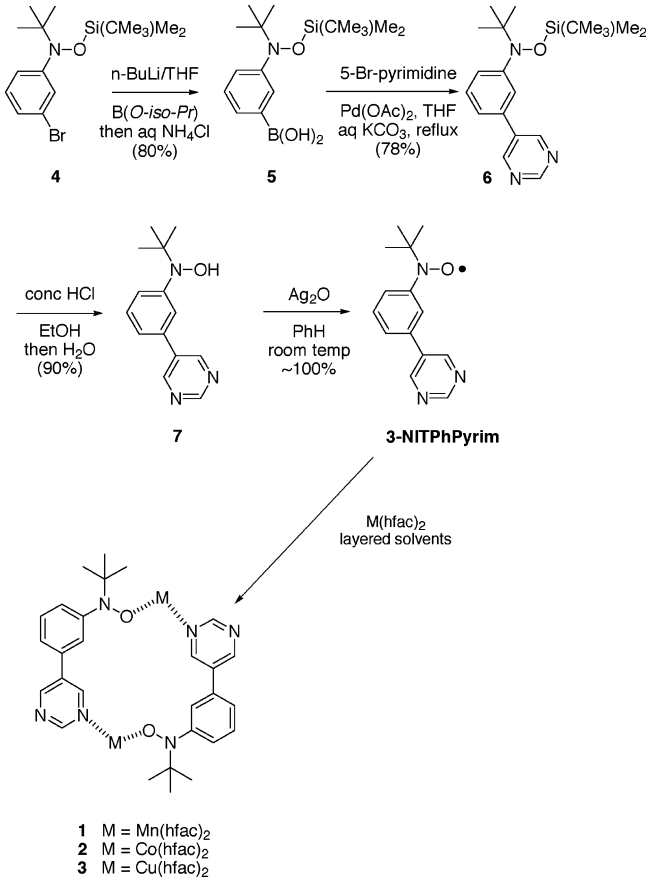

that was best used immediately after synthesis. The lower stability of 3NITPhPyrim by comparison to 4NITPhPyrim—which can be isolated[3b] as a stable solid—may be due to the fact that it is not sterically blockaded in the position *para* to the nitroxide unit, allowing increased reactivity at this position. Despite the limited stability of 3NITPhPyrim, its complexes made from carefully layered solutions with $M(hfac)_2$ (M = Mn, Co, Cu) were highly stable and readily characterized (Scheme 1). The Mn(II) and Co(II) coordinations yielded **1** and **2**, respectively, as the only isolated products. We had more difficulty in obtaining pure **3** in a reproducible fashion without other coordination side products. We have not carried out systematic study of the kinetics of formation of **3** by comparison to alternate coordination products, but its formation seems favored by very slow evaporation of less polar solvent mixtures in larger volumes.

(3) (a) Field, L. M.; Lahti, P. M.; Palacio, F. *Chem. Commun.* **2002**, 636. (b) Field, L. M.; Lahti, P. M.; Palacio, F.; Paduan-Filho, A. *J. Am. Chem. Soc* **2003**, *125*, 10110. (c) Field, L. M.; Lahti, P. M. *Inorg. Chem.* **2003**, *42*, 7447.
(4) Liao, Y.; Xie, C.; Lahti, P. M.; Weber, R. T.; Jiang, J.; Barr, D. P. *J. Org. Chem.* **1999**, *64*, 5176.
(5) Becke, A. D. *J. Chem. Phys.* **1993**, *98*, 5648.
(6) Frisch, M. J.; Trucks, G. W.; Schlegel, H. B.; Scuseria, G. E.; Robb, M. A.; Cheeseman, J. R.; Montgomery, J. A. J.; Vreven, T.; Kudin, K. N.; Burant, J. C.; Millam, J. M.; Iyengar, S. S.; Tomasi, J.; Barone, V.; Mennucci, B.; Cossi, M.; Scalmani, G.; Rega, N.; Petersson, G. A.; Nakatsuji, H.; Hada, M.; Ehara, M.; Toyota, K.; Fukuda, R.; Hasegawa, J.; Ishida, M.; Nakajima, T.; Honda, Y.; Kitao, O.; Nakai, H.; Klene, M.; Li, X.; Knox, J. E.; Hratchian, H. P.; Cross, J. B.; Adamo, C.; Jaramillo, J.; Gomperts, R.; Stratmann, R. E.; Yazyev, O.; Austin, A. J.; Cammi, R.; Pomelli, C.; Ochterski, J. W.; Ayala, P. Y.; Morokuma, K.; Voth, G. A.; Salvador, P.; Dannenberg, J. J.; Zakrzewski, V. G.; Dapprich, S.; Daniels, A. D.; Strain, M. C.; Farkas, O.; Malick, D. K.; Rabuck, A. D.; Raghavachari, K.; Foresman, J. B.; Ortiz, J. V.; Cui, Q.; Baboul, A. G.; Clifford, S.; Cioslowski, J.; Stefanov, B. B.; Liu, G.; Liashenko, A.; Piskorz, P.; Komaromi, I.; Martin, R. L.; Fox, D. J.; Keith, T.; Al-Laham, M. A.; Peng, C. Y.; Nanayakkara, A.; Challacombe, M.; Gill, P. M. W.; Johnson, B.; Chen, W.; Wong, M. W.; Gonzalez, C.; Pople, J. A. *Gaussian 03*, B03 ed.; Gaussian, Inc.: Pittsburgh, PA, 2003.

Table 1. Crystallographic Analysis Parameters for **1**−**3** at Varying Temperatures[a]

param	**1**	**2**	**3**
chem formula	$C_{48}H_{36}F_{24}Mn_2N_6O_{10}$	$C_{48}H_{36}F_{24}Co_2N_6O_{10}$	$C_{48}H_{36}F_{24}Cu_2N_6O_{10}$
fw	1422.7	1430.69	1439.91
cell setting, space group	triclinic, $P\bar{1}$	triclinic, $P\bar{1}$	triclinic, $P\bar{1}$
a, *b*, *c* (Å)	9.4570(2), 10.6507(2), 16.4342(5) {9.00800(10), 10.1214(2), 16.6591(3)}	9.4474(2), 10.6040(3), 16.4930(5) [9.2310(2), 10.3568(2), 16.4551(4)]	9.6557(2), 16.0424(3), 19.6212(4) [9.51840(10), 15.8656(2), 19.4793(3)] {9.44230(10), 15.7864(2), 19.4298(4)}
α, β, γ (deg)	79.5093(8), 85.0207(8), 65.3736(17) {79.5635(8), 86.6765(8), 69.2349(9)}	78.6172(9), 85.0945(10), 64.9927(14) [79.1122(8), 85.5223(9), 66.7499(10)]	76.6264(6), 81.6717(6), 82.5520(9) [76.6884(5), 81.6336(5), 82.0372(7)] {76.6127(6), 81.7446(6), 81.6369(8)}
V (Å^3)	1479.49(6) {1396.68(4)}	1467.92(7) [1419.38(5)]	2911.11(10) [2815.27(6)] {2769.31(7)}
Z	1	1	2
D_x (Mg/m^3)	1.618 {1.691}	1.6718 [1.674]	1.643 [1.699] {1.727}
radiatn type	Mo Kα	Mo Kα	Mo Kα
F(000)	712	716	1440
μ (mm^{-1})	0.561 {0.594}	0.700 [0.724]	0.867 [0.896] {0.911}
cryst color	yellow-brown plate	dark yellow needle	yellow needle
R_{unt}	0.0236 {0.0169}	0.0257 [0.0185]	0.0324 [0.0312] {0.0361}
completeness to 2θ	0.972 {0.989}	0.998 [0.985]	0.989 [0.990] {0.986}
H-atom treatment	Refxyz	Refxyz	Refxyz
goodness of fit on F^2	1.042{1.043}	1.052[1.060]	1.026[1.015] {1.029}
$\Delta\rho_{max}$, $\Delta\rho_{min}$ (e Å^{-3})	0.872, −0.637 {0.849, −0.576)}	0.867, −0.726 [0.646, −0.546]	0.808, −0.739 [1.554, −0.798] {1.053, −0.977}
R_1, wR_2 ($I > 2\sigma(I)$)	0.0971, 0.2514 {0.0417, 0.1020}	0.0882, 0.2212 [0.0526, 1297]	0.0793, 0.1932 [0.0667, 0.1579] {0.0522, 0.1234}
R_1, wR_2 (all)	0.1111, 0.2668 {0.0450, 0.1048}	0.1085, 0.2392 [0.0568, 0.1332]	0.1111, 0.2140 [0.0899, 0.1732] {0.0702, 0.1336}
temp (K)	293{100}	293 [173]	299 [173] {100}

[a] See final row in table.

Complexes **1**−**3** were analyzed by single-crystal X-ray diffraction at various temperatures from 100 to 300 K. All three complexes crystallize in the $P\bar{1}$ triclinic space group. Tables 1 and 2 show crystallographic and structural parameters from the analyses; further details are given in Supporting Information. Figure 1 shows structural diagrams[7] for the complexes at room temperature. Figure 2 summarizes temperature-dependent geometry changes found for the structure of **3**, which are described in more detail in the following section.

Polycrystalline samples of **1**−**3** were subjected to dc magnetic susceptibility studies using a Quantum Design MPMS-5 magnetometer. Samples were placed in gelatin capsules and held in place with cotton, and were analyzed from 1.8 to 300 K. Figures 3−5 show χT vs T plots obtained for **1**−**3** at 1, 0.1, and 1 T, respectively. Figure 4 also shows a $1/\chi$ vs T Curie−Weiss plot of the same data for **2**. Figure 5 also shows an inset of the same data for **3** as a χ vs T plot, to emphasize the loss of overall paramagnetic susceptibility as the temperature drops for this sample. The solid lines in the figures represent fits to the data for models that are discussed in detail below. Magnetization versus field measurements for **1**−**3** were carried out from 0 to 17 T and are compared for the three samples in Figure 6.

Discussion

Crystallography. Figure 1 shows that the complexes **1**−**3** all have similar room-temperature centrosymmetric geometries that incorporate 3NITPhPyrim = RL with the nitroxide group syn to the pyrimidine group. There is a limited torsion in the RL units: the Ph−NO torsions range from 9 to 24°, and the phenyl−pyrimidine torsions from 33 to 35°. The coordination environments around the metal centers are somewhat distorted from hexacoordinate octahedra, as shown by the bond angles in Table 2. A number of anti L−M−L angles range from 165 to 175° instead of 180°; other L−M−L angles range from 84 to 103° instead of 90°. In all of the structures, the pyrimidine unit is coordinated at an 83−86° angle relative to the nitroxide group, anti to an hfac carbonyl unit as was observed[3] in complexes of 4NITPh-Pyrim and 4NITPhTriaz.

The closest distance between metal ions in **1**−**3** is intradimeric, 7−7.5 Å; the closest intermolecular M···M distances are about 9−10 Å. With no close interdimer contacts between sites of significant spin density in the crystal structures of any of these complexes, the magnetic effects discussed in the following section are attributed to intramolecular exchange mechanisms. The crystallographic nitroxide and interannular torsions in the 3NITPhPyrim units seem not so large to preclude conjugation of the nitroxide into the π-system, which could contribute to intradimer spin polarization and exchange between the M−NIT spin units. But, the ESR spectrum of 3NITPhPyrim and the spin density computations described above show little spin density on the pyrimidine ring in the isolated radical. The coordinating metal ion could directly spin-polarize the pyrimidine ring, but previous studies suggest[3b] such polarization to be small.

There is only one molecule in the unit cells of **1** and **2**. Complex **3** has two similar but crystallographically distinct structures. The M−ON bond lengths in **1** and **2** are not greatly differentiated from the other M−O bond lengths, so axial versus equatorial distinctions for the nitroxide coordination is not strong. But, at room temperature, one molecule of **3** in the unit cell (form **3A**) shows strong Jahn−Teller

(7) Generated using ORTEP-III for Windows: Farrugia, L. J. *J. Appl. Crystallogr.* **1997**, *30*, 565.

Table 2. Selected Structural Parameters for **1**−**3** at Various Temperatures[a]

param	**1** (293 K)	**1** (100 K)	**2** (299 K)	**2** (173 K)	**3** (299 K)	**3** (173 K)	**3** (100 K)
M−ON	2.135(4)	2.139(2)	2.056(4)	2.058(2)	2.292(4) (A)	2.111(3) (A)	2.031(3) (A)
M−O(5)					2.166(4) (B)	2.002(3) (B)	1.984(3) (B)
			M−O Bond Lengths (hfac)				
M−O(1)	2.114(4)	2.116(2)	2.031(4)	2.031(2)	2.200(6)	2.062(5)	2.028(3)
					2.068(8)	1.991(4)	1.990(3)
M−O(2)	2.172(5)	2.179(2)	2.089(5)	2.093(2)	2.033(4)	2.165(4)	2.238(3)
					2.124(5)	2.254(4)	2.262(3)
M−O(3)	2.143(4)	2.148(2)	2.037(4)	2.037(2)	2.052(4)	2.212(4)	2.287(3)
					2.131(5)	2.293(4)	2.302(3)
M−O(4)	2.154(4)	2.144(2)	2.089(4)	2.083(2)	1.945(4)	1.921(3)	1.912(3)
					1.962(4)	1.949(3)	1.947(3)
			M−N Bond Length				
M(1)−N(pyri midine)	2.274(4)	2.253(2)	2.158(4)	2.148(2)	2.013(4)	2.001(4)	1.996(3)
					2.026(4)	2.005(4)	2.008(3)
			N−O Bond Length				
O(5)−N(1)	1.308(6)	1.302(2)	1.315(6)	1.303(3)	1.296(5)	1.295(5)	1.300(4)
					1.292(6)	1.298(5)	1.301(4)
			M···M Intradimer Distance				
M(1)···M(1)	7.491	7.446	7.371	7.327	7.111	6.986	6.952
					7.570	7.376	7.339
			Phen−NO Torsion				
O(5)−N(1)−C(17)−C(16)	19.79	19.57	20.11	19.79	12.20	10.09	9.15
					23.76	21.75	20.68
			Phen−Pyrim Torsion				
C(16)−C(15)−C(14)−C(11)	36.52	32.84	34.79	34.39	34.72	35.65	34.84
					32.91	33.47	32.63
			Angles				
O(1)−M−O(3)	166.21(18)	163.00(6)	170.41(18)	169.22(9)	170.16(17)	166.70(14)	164.99(10)
					172.2(2)	171.93(14)	172.16(10)
O(4)−M−N(2)	163.23(16)	161.92(7)	170.83(17)	170.80(9)	173.20(18)	174.15(16)	173.82(12)
					173.2(2)	173.22(15)	173.14(12)
O(5)−M−O(2)	167.28(15)	163.00(6)	173.28(16)	171.77(8)	174.40(16)	175.01(15)	175.63(11)
					178.00(19)	177.47(14)	177.66(11)
O(5)−M−O(3)	103.71(16)	106.10(6)	100.05(16)	101.22(9)	100.57(16)	102.19(13)	102.80(10)
					94.59(18)	94.92(14)	95.18(10)
O(5)−M−N(2)	85.10(15)	84.13(6)	84.46(17)	84.48(9)	85.50(16)	86.43(14)	86.40(11)
					83.15(17)	83.79(14)	83.54(11)

[a] See Figure 1 for atom numbering. All distances in angstroms, all angles in degrees.

elongation of the coordinated nitroxide Cu(1)−O(5)N bond (2.29 Å) and the anti-related Cu(1)−O(1) hfac bond (2.2 Å); the other, equatorial Cu(II)−O(hfac) bond lengths range from 1.99 to 2.03 Å. Form **3B** is less distorted, with the Cu(2)−O(5a)N bond being longest by 0.03 Å among four M−O bond lengths ranging from 2.07 to 2.17 Å. Save for the different bond lengths, the coordination spheres and conformational geometries of the two molecules of **3** are analogous.

The variable-temperature crystallographic analyses were important to show the differences in behavior among these compounds. Mn(II) complex **1** showed no significant molecular structural changes upon cooling, although the unit cell undergoes an approximately 0.5 Å contraction of the *a*- and *b*-axes with slight elongation of the *c*-axis and a unit cell volume contraction of only 6.5%. Co(II) complex **2** similarly showed no significant molecular structural changes upon cooling, with only a 3.4% contraction of the unit cell volume down to 173 K, at which temperature all crystals studied broke, presumably as a result of some sort of phase change.

Cu(II) complex **3** differs from **1** and **2** by having two crystallographically distinct forms that exhibit coordination sphere bond length changes of up to 0.26 Å upon cooling to 100 K, during which its unit cell volume decreases by 4.9% (see Tables 1 and 2). Figure 2 summarizes the coordination sphere changes around the Cu(II) ions. The Cu−ON bonds in both forms of **3**, which are elongated at room temperature, contract markedly by 100 K, as do the anti-related Cu−O(hfac) bonds; there is also a small contraction of the Cu−N bonds and their anti-related Cu−O(hfac) bonds. Simultaneously, the remaining anti-related pair of Cu−O(hfac) bonds elongates significantly. These geometric changes are reversible upon rewarming the sample. This corresponds to a change from an axial environment at room temperature to an equatorial environment at 100 K for the Cu−ON bond and its anti-related Cu−O(hfac) bond. This is very important for explaining the magnetic behavior of **3** that is described below.

Magnetism and Spectroscopy. Neither of complexes **1** and **2** showed an X-band TE102 mode ESR spectrum in the solid state at either room temperature or 77 K. Any ESR spectral transitions are apparently either too weak or too broad to observe under these conditions. Complex **3** shows a weak and broadened peak at 77 K at $g = 2.06$ versus DPPH standard.

The magnetic measurements for the high-temperature region of manganese complex **1** yield a Curie constant of $C = 5.8$ emu-K/(Oe-mol), in good accord with the value of

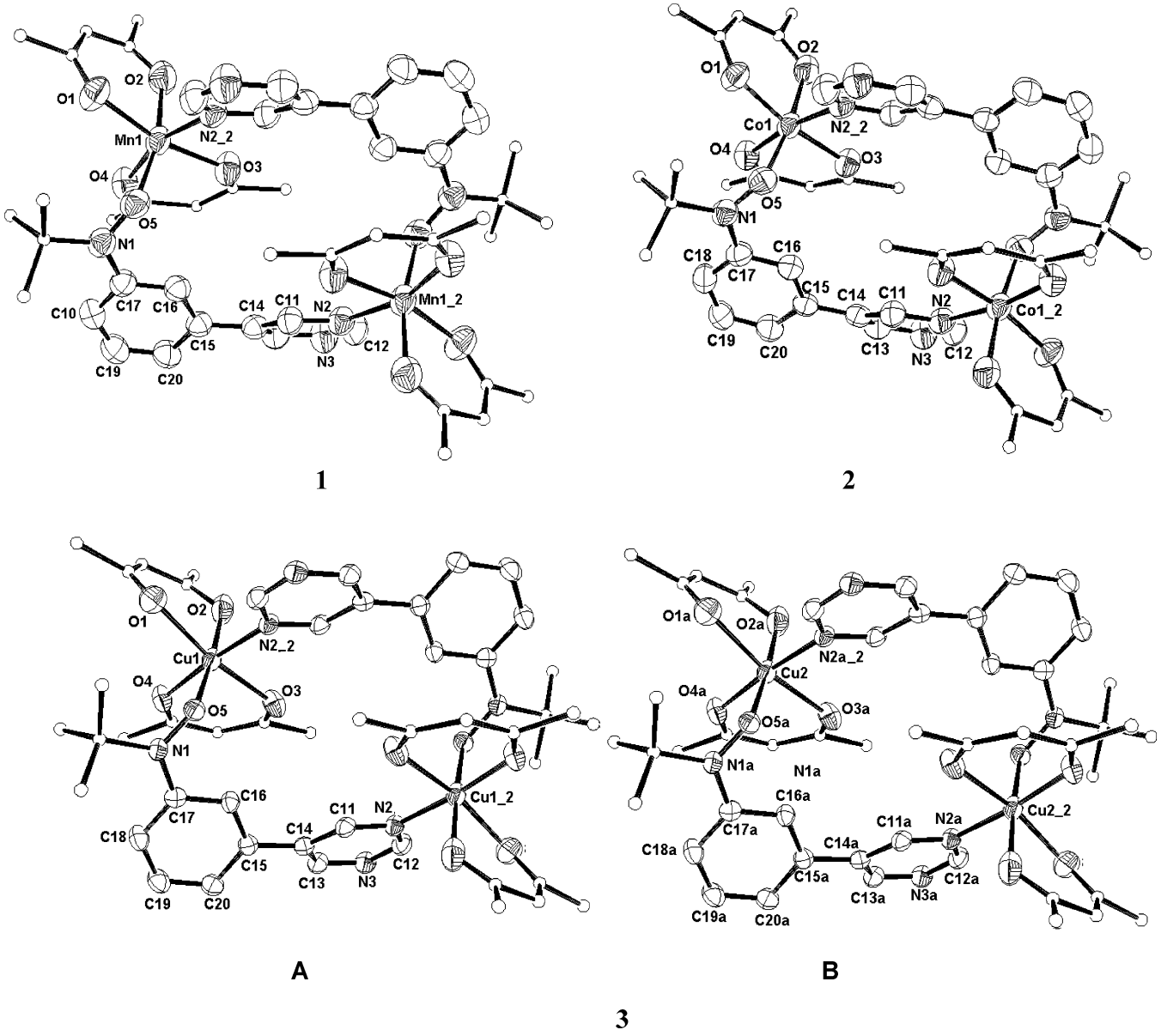

Figure 1. ORTEP style structures of **1**−**3** showing 50% probability ellipsoids, with atom numbering used in the main text. Hydrogen and fluorine atoms are omitted for clarity of viewing. Structure **3** has two similar but crystallographically distinct forms, A and B.

6.0 emu-K/(Oe-mol) expected for a dimer of $S = 4/2$ units that arise from antiferromagnetic (AFM) Mn(II) to radical exchange. The magnetization versus field plot for **1** at 1.4 K (Figure 6) saturates at $M(H) = 8.0\ \mu_B$/mol, also appropriate for a dimer of $S = 4/2$ spin units. Since all of the d-orbitals of octahedral Mn(II) are singly occupied, overlap with the nitroxide SOMO ensures AFM exchange.[1a,b,j] The slow initial rise of the χT versus T plot and the rapid decrease below 20 K (Figure 3) suggest multiple exchange mechanisms.

A rectangular four-spin fit to the magnetic data was carried out using the program MAGMUN,[8] varying the effective Lande factor g_{eff}, and using two exchange constants J_1/k and J_2/k plus a temperature-independent paramagnetic contribution TIP. No zfs or spin−orbit effects were included in the estimation procedure. A similar procedure has been described for a $Mn_2(RL)_2$ type dimer by Rabu et al.[2e] Figure 3 shows a good fit to the data for **1** with $g_{eff} = 1.97$, $J_1/k = (-)790$ K $= (-)550$ cm^{-1}, $J_2/k = (+)1.0$ K $= (+)0.7$ cm^{-1}, and TIP $= (-)0.0019$ emu/(Oe-mol). The strongly AFM exchange occurs within the Mn(II)−ON bond (based on the Curie constant described above), with the weak ferromagnetic (FM) exchange assigned to interaction between the Mn(II)−ON units, presumably in an intramolecular fashion due to a lack of close crystallographic contacts between Mn(II)−ON units.

A spin polarization mechanism analogous to those applied to the complexes of 4NITPhPyrim and 4NITPhTriaz[3b−c] is consistent with the FM exchange between the Mn(II)−ON spin units (Scheme 2). But, the results show that the intradimer FM exchange mechanism between Mn(II)−ON units in **1** is quite weak, probably due to the difficulty of

(8) MAGMUN is an integrated Windows-based software package for the solution of magnetic exchange problems. It was written by Dr. Zhiqiang Xu in collaboration with Prof. L. K. Thompson and Dr. O. Waldmann. A copy may be obtained from http://www.ucs.mun.ca/~lthomp/magmun.html.

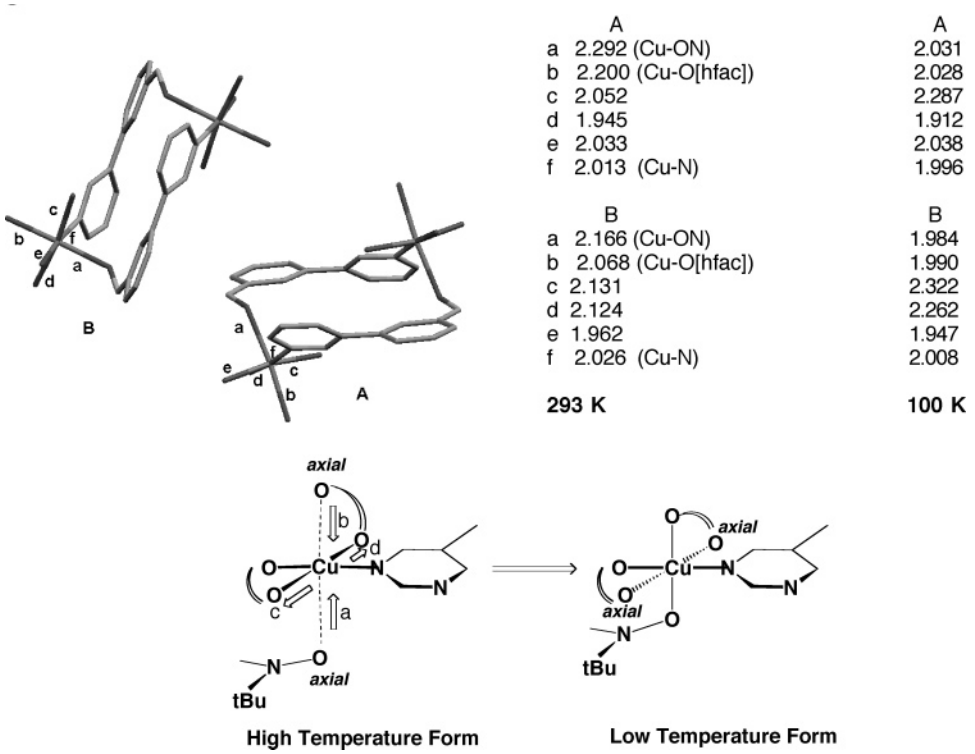

Figure 2. Geometric deformations observed for the two forms of **3** upon cooling. Bond lengths given in Å. Axial bonds in the schematic are correlated with longer bond lengths; the arrows in the high-temperature picture show the elongation/contraction of bonds in the **3A** form with cooling.

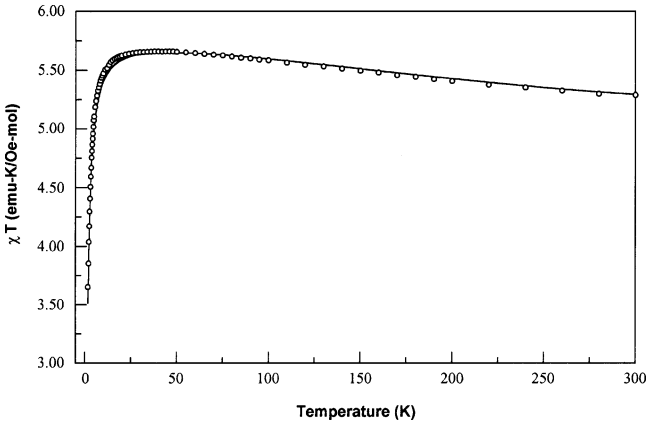

Figure 3. χT versus T plot for **1** at 1 T. The solid line shows a rectangular four-spin fit described in the text.

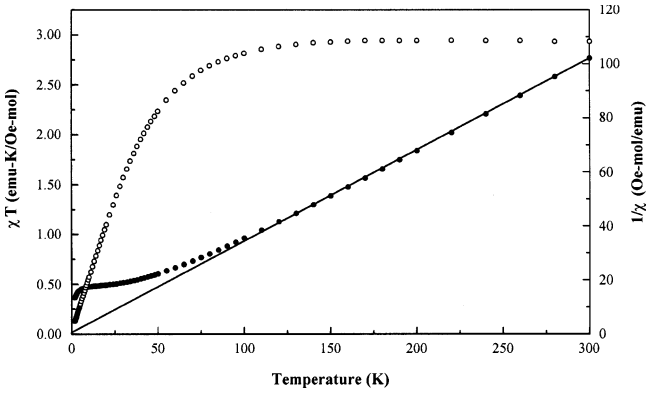

Figure 4. χT versus T (○) and $1/\chi$ versus T plots (●) for **2** at 0.1 T. The solid line shows a Curie−Weiss fit to $1/\chi$ versus T over 1.8−300 K.

transmitting spin polarization from the phenyl nitroxide unit through the pyrimidine unit in the 3NITPhPyrim ligands.

Interestingly, we found no evidence of a discontinuity in the χT versus T plot for polycrystalline cobalt complex **2** at about 170 K (Figure 4), the temperature below which single crystals of **2** fractured, as mentioned earlier. The lack of magnetic sensitivity to the presumed phase change that causes the fracture supports the assumption that intramolecular effects dominate the magnetism of **2**. At 100 K and higher, the $\chi T(T)$ data plateau at $C \sim 3$ emu-K/(Oe-mol). A Curie−Weiss fit to $1/\chi(T)$ above 120 K yields $C = 2.96$ emu-K/(Oe-mol) and $\theta = (-)1.7$ K (Figure 4). Typically, each octahedral Co(II) contributes[9] ~3.2 emu-K/(Oe-mol) to χT, so two Co(II) ions plus two nitroxides should give $\chi T \sim 7$ emu-K/(Oe-mol), much higher than observed. But, using the relationship $C = 0.125(g_{\text{eff}})^2 S(S + 1)$, a dimer of $S = 2/2$ spin units with $g_{\text{eff}} = 2.45$ would give $C = 3.0$ emu-K/(Oe-mol), in good agreement with the observed value. This shows strong AFM exchange in the Co(II)−NIT units to give effective $S = (3/2)-(1/2)$. The deviation from the free electron value of the Landé constant is not atypical for octahedral Co(II).[9]

Below 100 K, $\chi T(T)$ for **2** drops steadily to 0.13 emu-K/(Oe-mol) at 1.8 K. AFM spin pairing in the Co−ON unit makes them effectively $S \sim 0$ with loss of paramagnetic moment at low temperature. However, paramagnetic states are still accessible at high field. $M(H)$ at 1.4 K rises monotonically to the maximum measured field of 17 T, without giving a plateau (Figure 6). The maximum effective magnetization is about 2 μ_B, about half the value expected for two $S = 2/2$ units in the dimer. The overall results show

(9) Carlin, R. L. *Magnetochemistry*; Springer-Verlag: Berlin, 1986; pp 65−67.

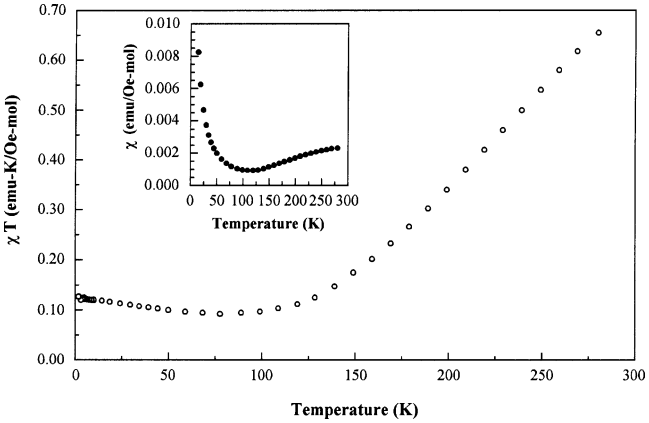

Figure 5. χT versus T plot for **3** at 1.0 T. (The inset shows the same data, χ versus T.)

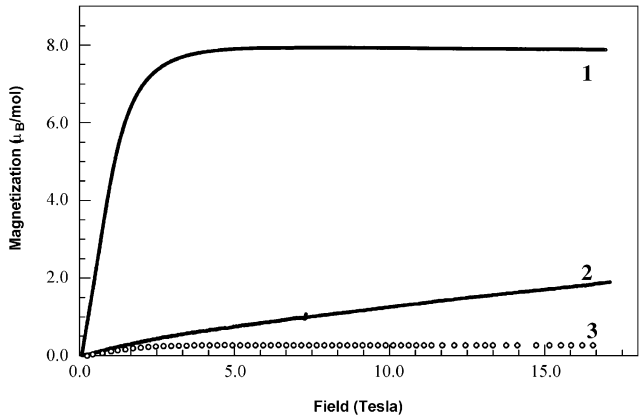

Figure 6. Magnetization versus field measurements for **1** (1.4 K), **2** (1.4 K), and **3** (1.2 K).

Scheme 2. Qualitative Spin Polarization Mechanism for Intramolecular FM Exchange in **1**

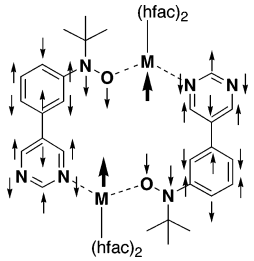

a strong AFM exchange within the Co(II)−NIT units but do not readily allow extraction of the intradimer exchange energy between the Co(II)−NIT units due to the complexity of Co(II) magnetic behavior by comparison to **1**.

For copper complex **3**, a noninteracting set of four $S = 1/2$ spins should give a high-temperature χT plateau corresponding to a Curie constant of $C \sim 1.5$ emu-K/(Oe-mol). Two strongly FM coupled $S = 1$ Cu(II)−ON units in the dimer should give $C \sim 2.0$ emu-K/(Oe-mol). However, χT(300 K) $\sim$ 0.7 emu-K/(Oe-mol) and decreases steadily from 300 to 100 K. There is no higher temperature plateau (Figure 5). At 100 K, χT reaches a minimum value of 0.10 emu-K/(Oe-mol) and then weakly increases to 0.13 emu-K/(Oe-mol) at 1.8 K. The paramagnetic susceptibility χ also decreases from 300 to 100 K. This behavior is virtually the same at both 0.01 and 1.0 T. The magnetization versus field plot of **3** at 1.25 K shows only a small saturation moment above 4 T.

Scheme 3. Qualitative Spin−Orbital Overlap Diagram Showing Essentially Zero Overlap of Nitroxide SOMO of 3NITPhPyrim with Cu(II) SOMO in Axial Coordination at Higher Temperature but Significant Overlap in Equatorial Coordination at Lower Temperature

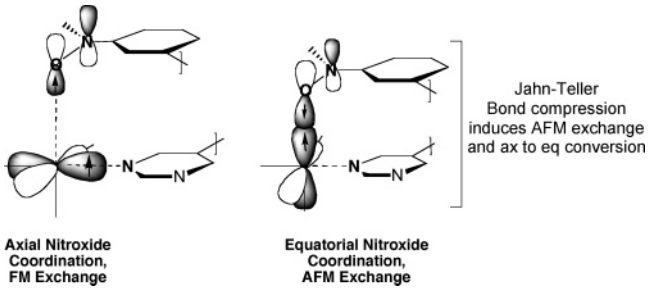

On the basis of the low value of χT at room temperature, there must be significant AFM exchange between spins in the sample of **3**. The AFM coupling is presumably strongest in the molecules of **3** in the unit cell having the shorter Cu(II)−ON bonds. The decrease in χT with temperature correlates with the shortening of all the Cu(II)−ON bonds upon cooling, during which the magnetic moment disappears save for a remnant (Figure 6) that is likely due to crystal defect paramagnetic sites or other small paramagnetic impurities that are below the limits detectable by elemental analysis. The lower temperature χT rise is not due to spin canting, since the saturation magnetization of the sample quickly plateaus at only a few percent of the total possible spins in the sample for fields up to 17 T.

Axial elongation of the Cu(II)−ON bonds yields FM Cu(II)−ON exchange due to the orthogonality of the Cu(II) axial SOMO with the nitroxide SOMO. Shortening the Cu(II)−ON bond leads to SOMO−SOMO overlap and AFM exchange, as the nitroxide changes to equatorial coordination (Scheme 3).[1a−c,10] The molecule of **3** in the unit cell that has less Jahn−Teller distortion at room temperature is part way along the axial to equatorial Cu(II)−ON changeover and presumably is responsible for the reduced moment of **3** at 300 K relative to the value expected. As a result **3** exhibits a strongly temperature-modulated magnetic moment, as two different structural contributors to the moment separately undergo changes in Cu(II)−ON exchange strength.

The magnetic and structural changes in copper complex **3** are accompanied by a strong thermochromic change. At room temperature, **3** is a dull yellowish-brown solid. Upon cooling, it becomes progressively more greenish, yielding a bright lime green at 77 K. This thermochromism is reversible over as many cycles as we have tested. It seems clear that the green color is associated with the low-spin state and a strongly AFM exchange coupled Cu−ON bond, while the yellow-brown color is associated with the high-spin or poorly exchange coupled Cu(II)−ON state.

(10) (a) Caneschi, A.; Gatteschi, D.; Rey, P. *Prog. Inorg. Chem.* **1991**, *39*, 331. (b) Luneau, D.; Rey, P.; Laugier, J.; Fries, P.; Caneschi, A.; Gatteschi, D.; Sessoli, R. *J. Am. Chem. Soc.* **1991**, *113*, 124. (c) Ressouche, E.; Boucherle, J.-X.; Gillon, B.; Rey, P.; Schweizer, J. J. *J. Am. Chem. Soc.* **1993**, *115*, 3610. (d) Boucherle, J.-X.; Ressouche, E.; Schweizer, J.; Gillon, B.; Rey, P. *Z. Naturforsch.* **1993**, *48*, 120.

Table 3. Comparison of Selected Structural Parameters for **3** (100 K) and **8** (293 K)[a]

	3 (100 K)	**8** (293 K)
Cu-ON(a) bond length	2.031(3) A 1.984(3)[a] B	1.9776(13)
Cu-O bond lengths (hfac)		
Cu-O(b)	2.028(3) 1.990(3)	2.0142(13)
Cu-O(c)	2.238(3) 2.262(3)	2.3735(12)
Cu-O(d)	2.287(3) 2.302(3)	2.3542(13)
Cu-O(e)	1.912(3) 1.947(3)	1.9351(11)
Cu-N (f) bond length	1.996(3) 2.008(3)	1.9776(13)
N-O bond length	1.300(4) 1.301(4)	1.2952(17)
Cu----Cu intradimer distance	6.952 7.339	6.915
Phen-NO torsion	9.15 20.68	10.68
Phen-Pyrim torsion	34.84 32.63	37.54
Angles		
O-Cu-O (c-d)	164.99(10) 172.16(10)	155.05(5)
O-Cu-N (f-e)	173.82(12) 173.14(12)	173.83(5)
O-Cu-O(N) (a-b)	175.63(11) 177.66(11)	174.01(5)
O-Cu-O(N) (d-a)	102.80(10) 95.18(10)	101.05(5)
(N)O-Cu-N (a-f)	86.40(11) 83.54(11)	92.63(5)

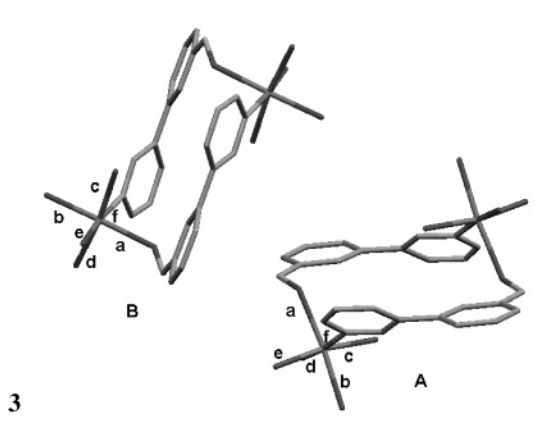

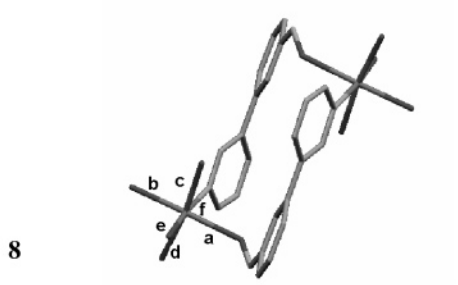

[a] Letters in table refer to accompanying figures.

We were also able to test the effect of forming a short, strong Cu(II)−ON bond in this type of $Cu_2(RL)_2$ system by making model complex **8**. Radical 3NITPhPyr was synthesized by replacing 5-bromopyrimidine with 3-bromopyridine in the route of Scheme 1. Cyclic **8** was then obtained after some effort by crystallization of 3NITPhPyr with $Cu(hfac)_2$ using procedures similar to those used to make **3**. There was only one structure of **8** in the crystal lattice. It has conformation and torsions of the radical ligand portion similar to those for the structures of **3**, as well as other geometric parameters (Table 3). Details are given in the Supporting Information and the Experimental Section.

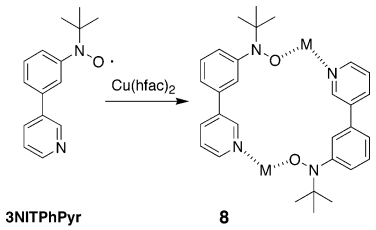

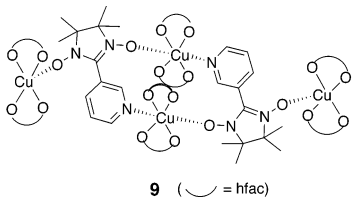

Notably, at room temperature the Cu(II)−ON bonds and the anti-related Cu−O(hfac) bonds in **8** are already shortened by comparison to the room-temperature structures of **3**. The room-temperature structure of **8** is thus analogous to the *low-temperature* form of **3**, as shown in Table 3. At temperatures down to 1.8 K, **8** showed no appreciable paramagnetic susceptibility, showing strongly AFM Cu(II)−ON exchange. The correlation of short Cu−ON bond lengths with strong AFM exchange in **8** is consistent with the interpretation given above for the magnetostructural variation of **3** as a function of temperature. Interestingly, low-spin complex **8** is green even at room temperature, consistent with the above-described green color of the low-temperature, low-spin state of complex **3**.

In work closely related to ours, Lanfranc de Panthou et al.[11] described a study of complex **9**, a cyclic dimer end-capped with Cu(II) ions. Upon cooling, the complex exhibited Cu(II)−ON bond shortening of ∼0.2 Å in the dimeric portion with a drop in χT from 2.5 to 0.8 emu-K/(Oe-mol) over the 150−100 K temperature range, corresponding to a

(11) Lanfranc de Panthou, F.; Belorizky, E.; Calemczuk, R.; Luneau, D.; Marcenat, C.; Ressouche, E.; Turek, P.; Rey, P. *J. Am. Chem. Soc.* **1995**, *117*, 11247.

change from six to two isolated $S = 1/2$ units. These workers pointed out that shortening the Cu(II)−ON bonds changed the nitroxide coordination from axial to equatorial, giving a loss of magnetic moment in the dimeric portion of the structure for the reasons exemplified in Scheme 3. They described this behavior as a thermally induced spin conversion[11] (as opposed to a spin crossover, which is mechanistically distinct[12]). Ovcharenko[13] has also recently described a series of coordination complexes derived from $Cu(hfac)_2$ and one nitronyl nitroxide radical, some of which show temperature-dependent bond length changes that modulate magnetic moment.

Conclusions

Dimers **1** and **2** show quite strong AFM metal ion to nitroxide exchange, which is consistent with the strong overlap between spin-bearing orbitals. A weak FM exchange observed in **1** between Mn−NIT spin sites is in accord with expectations of a spin polarization model. The metal ion to nitroxide exchange in copper complex **3** is variable due to a thermally reversible Jahn−Teller distortion of the Cu(II) coordination sphere in two crystallographically different molecules, which leads to conversion from ferromagnetic (high-temperature) to antiferromagnetic (low-temperature) Cu(II)−NIT coupling. Complex **3** also shows a strong thermochromic and magnetochromic effect that correlates qualitatively with changes in its magnetic behavior as a function of temperature. This thermally induced spin state change allows possibilities for modulating the magnetic moments and optical properties of compounds that contain **3** by modulating the temperature.

Experimental Section

General Procedures. Reactions were carried out in oven-dried glassware, under an argon atmosphere. 2-Methyl-2-nitrosopropane was prepared according to the procedure of Stowell.[14] Diethyl ether and tetrahydrofuran (THF) were distilled under argon after drying over sodium. Dri-Solv *N*,*N*-dimethylformamide (DMF) was obtained from EM Science and used without further purification. Other chemicals were purchased from Acros, Avocado, and Aldrich Chemical Cos. Diethyl ether was distilled under argon after drying over sodium. Hexanes were distilled under argon after drying over calcium hydride.

3-Bromo-*N*-*tert*-butylamino-*N*-*tert*-butyldimethylsiloxylbenzene (4). A solution of 1.5 M *n*-butyllithium in hexanes (11.3 mL, 17.0 mmol) was added to a solution of 1,3-dibromobenzene (4.00 g, 17.0 mmol) in 80 mL of diethyl ether under argon at −78 °C. The suspension was allowed to stir for 30 min, warmed to room temperature at which time it went into solution, and then cooled to −78 °C. A solution of 2-methyl-2-nitrosopropane[14] (2.22 g, 25.4 mmol) in diethyl ether (15 mL) was added, and the reaction was left to stir overnight at ambient temperature. Aqueous saturated ammonium chloride (25 mL) was added, and then the organic layer was separated and washed with water. The aqueous layer was extracted with diethyl ether, and the combined organic layers were dried over magnesium sulfate. Evaporation of the solvent yielded pale yellow crystals of 3-bromo-*N*-*tert*-butyl-*N*-hydroxylaminobenzene that were dried under vacuum and used immediately in the next step (see ref 4).

The crystals from the previous step were dissolved in 20 mL of dry DMF and then added to a mixture of *tert*-butyldimethylchlorosilane (5.11 g, 33.9 mmol) and imidazole (3.46 g, 50.8 mmol) in a predried flask. The resulting solution was stirred under argon for 24 h at 50 °C. Distilled water (20 mL) was added, and the solution was extracted with hexanes. The combined organic layers were dried over magnesium sulfate and evaporated under reduced pressure. Purification by column chromatography on silica gel with hexanes yielded 5.35 g (89%) of **4** as a clear colorless oil that is spectroscopically identical to that previously reported in ref 4. This material can be used directly in the next synthetic step. ^{1}H NMR (200 MHz, $CDCl_3$): δ −0.12 (broad s, 6 H), 0.90 (s, 9 H), 1.09 (s, 9 H), 7.04−7.24 (m, 3 H), 7.43 (s, 1 H).

(*N*-*tert*-Butyl-*N*-(*tert*-butyldimethylsiloxy)amino)phenyl-3-boronic Acid (5). A solution of 1.54 M *n*-butyllithium in hexanes (3.9 mL, 6.0 mmol) was added dropwise to a solution of **4** (2.17 g, 6.05 mmol) in 40 mL of THF under argon at −78 °C. The reaction was allowed to stir for 1.5 h. Next, triisopropyl borate (1.75 mL, 7.57 mmol, Avocado Research Chemicals) was added via syringe, and the reaction was allowed to warm to room temperature overnight. Aqueous ammonium chloride (5 mL) was added, and the reaction was allowed to stir for 1 h. The organic layer was separated and washed with brine. The combined aqueous portions were extracted with diethyl ether. The combined organic portions were dried over anhydrous magnesium sulfate and evaporated under reduced pressure. Purification by column chromatography (silica gel, 7:3 ethyl acetate−hexanes) yielded 1.57 g (80%) of **5** as a colorless crystalline powder, mp 49−50 °C. This product can be used as is in the subsequent step. ^{1}H NMR (300 MHz, $CDCl_3$): δ −0.10 (broad s, 6 H), 0.96 (s, 9 H), 1.15 (s, 9 H), 7.37 (d, 1 H, J = 7.22 Hz), 7.46 (broad s, 1 H), 7.94 (d, 1 H, J = 7.22 Hz), 8.09 (broad s, 1 H).

5-[3-(*N*-*tert*-Butyl-*N*-(*tert*-butyldimethylsiloxyl)amino)phenyl]-pyrimidine (6). A flask charged with 5-bromopyrimidine (0.477 g, 3.00 mmol) and palladium(II) acetate (0.0350 g, 0.156 mmol) was evacuated and backfilled with argon three times. Tetrahydrofuran (10 mL) was added, and the suspension was allowed to stir for 10 min. Deaerated solutions of boronic acid **5** (1.26 g, 3.89 mmol) in THF (5 mL) and of potassium carbonate (1.03 g, 7.48 mmol) in distilled water (4.5 mL) were added via cannula. The stirring reaction was heated to reflux for 24 h under argon. The organic layer was separated. The aqueous layer was extracted with diethyl ether. The combined organic portions were dried over magnesium sulfate and evaporated under reduced pressure. Purification by column chromatography (silica gel, 8:2 hexanes−ethyl acetate) yielded 0.83 g (78%) of **6** as a white crystalline powder. Recrystallization in hexanes yielded clear colorless needle crystals, mp 119−120 °C. ^{1}H NMR (300 MHz, $CDCl_3$): δ −0.10 (broad s, 6 H), 0.93 (s, 9 H), 1.14 (s, 9 H), 7.30−7.41 (m, 3 H), 7.51 (broad s, 1 H), 8.93 (s, 2 H), 9.20 (s, 1 H). Anal. Calcd for $C_{20}H_{31}ON_3Si$: C, 67.18; H, 8.74; N, 11.75. Found: C, 67.24; H, 8.76; N, 11.81.

5-[3-(*N*-*tert*-Butyl-*N*-hydroxylamino)phenyl]pyrimidine (7). Concentrated HCl (1 mL) was added to a solution of **6** (0.367 g, 1.03 mmol) in ethanol (5 mL). The solution was allowed to stir under argon overnight, concentrated under vacuum, and then diluted with distilled water (5 mL). The resulting solution was brought to pH 5 with 1 M sodium hydroxide and extracted with dichlo-

(12) For a recent example, see: Sunatsuki, Y.; Ohta, H.; Kojima, M.; Ikuta, Y.; Goto, Y.; Matsumoto, N.; Iijimi, S.; Akashi, H.; Kaizaki, S.; Dahan, F.; Tuchagues, J.-P. *Inorg. Chem.* **2004**, *43*, 4154. See also cited work in this reference.

(13) Fokin, S.; Ovcharenko, V.; Romanenko, G.; Ikorski, V. *Inorg. Chem.* **2004**, *43*, 969.

(14) Stowell, J. C. *J. Org. Chem.* **1971**, *36*, 3055.

romethane. The combined organic portions were dried over magnesium sulfate and evaporated under reduced pressure and then dried under vacuum and ground up to yield 0.225 g (90%) of pale yellow crystalline powder **7**, mp 126−128 °C. ^{1}H NMR (200 MHz, $CDCl_3$): δ 1.18 (s, 9 H), 7.32−7.45 (m, 4 H), 8.91 (s, 2 H), 9.19 (s, 1 H). IR (KBr disk, cm^{-1}): 3233 (N−OH). HRMS EI: calcd for $C_{14}H_{17}ON_3$, $[M + H]^+$ 243.1372; found, 243.1344. The structure was confirmed by crystallographic analysis (see Supporting Information). The crystal and structural parameters in CIF format were deposited at the Cambridge Crystallographic Databank Center, CCDC Deposition No. 234245.

5-[3-(*N*-*tert*-Butyl-*N*-aminoxyl)phenyl]pyrimidine (3NITPhPyrim). To a stirred solution of 5-[3-(*N*-*tert*-butyl-*N*-hydroxylamino)phenyl]pyrimidine, **7** (0.223 g, 0.917 mmol), in benzene (20 mL) under argon was added Ag_2O (0.531 g, 2.29 mmol). After 2 h the reaction was filtered to yield a clear red/orange solution. This was used directly for spectroscopic studies and as a reactant in subsequent reactions. The radical is not stable to prolonged storage and so is best used as soon as possible after preparation. ESR (benzene, room temperature, 9.649 GHz): a_N = 12.28 G; a_H = 2.03, 1.92, 1.82, 0.83 G; correlation 0.996 for fitting with Duling's WINSIM program.[15]

$Mn_2(hfac)_4$(3NITPhPyrim)$_2$ (1). 3NITPhPyrim **(**0.010 g, 0.041 mmol) was dissolved in 0.1 mL of dichloromethane, and then a solution of $Mn(hfac)_2$ (0.019 g, 0.041 mmol) dissolved in 0.2 mL of diethyl ether plus 1.0 mL of hexanes was layered on top. Yellow-brown plates formed after several days, mp 168−169.5 °C. Anal. Calcd for $C_{48}H_{36}O_{10}N_6F_{24}Mn_2$: C, 40.52; H, 2.55; N, 5.91. Found: C, 40.72; H, 2.69; N, 5.78. Crystallographic analysis was carried out on a Bruker P4 at ambient temperature with Mo Kα radiation: λ = 0.7107 Å, μ(Mo Kα) = 0.561 mm^{-1}; yellow-brown plate crystals 0.75 × 0.50 × 0.15 mm; formula $C_{48}H_{36}F_{24}Mn_2N_6O_{10}$ (fw 1422.7); triclinic space group $P\bar{1}$; cell parameters a = 9.4570(2) Å, b = 10.6507(2) Å, c =16.4342(5) Å, α = 79.5093(8)°, β = 85.0207(8)°, γ = 65.3736(17)°, V = 1479.49(6) Å^3, Z = 2; D_{calc} = 1.597 g/cm^3. N = 5086 unique reflections were measured using ω scans for 4.25 < θ < 25.05. The structure was solved by direct methods and refined on F^2 for all reflections with $I > 2\sigma(I)$ using 406 parameters and full-matrix least squares in SHELXTL97[15] to yield the structure with R_1 = 0.0971 and wR_2 = 0.2514; for all data, R_1 = 0.1111 and wR_2 = 0.2668. The crystal and structural parameters in CIF format were deposited at the Cambridge Crystallographic Databank Center, CCDC No. 272166.

$Co_2(hfac)_4$(3NITPhPyrim)$_2$ (2). 3NITPhPyrim (0.0600 g, 0.247 mmol) was dissolved in 1.5 mL benzene, and a solution of 0.117 g (0.247 mmol) of $Co(hfac)_2$ in 2 mL of distilled diethyl ether and 5 mL of hexanes was layered on top. This was then layered again with 5 mL of hexanes. After 4 days dark yellow needles formed, mp 165−167 °C. Anal. Calcd for $C_{48}H_{36}O_{10}N_6F_{24}Co_2$: C, 40.29; H, 2.54; N, 5.87. Found: C, 40.27; H, 2.57; N, 5.92. Crystallographic analysis was carried out on a Bruker P4 at ambient temperature with Mo Kα radiation: λ = 0.7107 Å, μ(Mo Kα) = 0.561 mm^{-1}; dark yellow needle crystals 0.75 × 0.20 × 0.02 mm; formula $C_{48}H_{36}Co_2F_{24}N_6O_{10}$ (fw 1430.69); triclinic space group $P\bar{1}$, cell parameters a = 9.4474(2) Å, b = 10.6040(3) Å, c = 16.4930(5) Å, α = 78.6172(9)°, β = 85.0945(10)°, γ = 64.9927(14)°, V = 1467.92(7) Å^3, Z = 1; D_{calc} = 1.645 g/cm^3. N = 5122 unique reflections were measured using ω scans for 4.14 < θ < 25.01. The structure was solved by direct methods and refined on F^2 for all reflections with $I > 2\sigma(I)$ using 406 parameters and full-matrix least squares in SHELXTL97[15] to yield the structure with R_1 = 0.0882 and wR_2 = 0.2212; for all data, R_1 = 0.1085 and wR_2 = 0.2392. The crystal and structural parameters in CIF format were deposited at the Cambridge Crystallographic Databank Center, CCDC No. 272167.

$Cu_2(hfac)_4$(3NITPhPyrim)$_2$ (3). 3NITPhPyrim (0.223 g, 0.917 mmol) was dissolved in 6.5 mL of dichloromethane, and then a solution of $Cu(hfac)_2$ (0.454 g, 0.917 mmol) in 6.0 mL of dichloromethane and 14.0 mL of hexanes was layered on top. After 1 week, a mixture of brown-green and light green crystals formed that was separated manually. The light green crystals were dissolved in toluene and filtered into a small vial. After 2 weeks fine needle crystals formed, mp 104−106 °C. Anal. Calcd for $C_{48}H_{36}O_{10}N_6F_{24}Cu_2$: C, 40.03; H, 2.52; N, 5.84. Found: C, 40.06; H, 2.28; N, 5.87. ESR (solid, 77 K): g = 2.06. Crystallographic analysis was carried out on a Bruker P4 at ambient temperature with Mo Kα radiation: λ = 0.7107 Å, μ(Mo Kα) = 0.561 mm^{-1}; yellow plate crystals 1.00 × 0.75 × 0.10 mm; formula $C_{48}H_{36}Cu_2F_{24}N_6O_{10}$ (fw 1439.91); triclinic space group $P\bar{1}$, with a = 9.6557(2) Å, b = 16.0424(3) Å, c = 19.6212(4) Å, α = 76.6264(6)°, β = 81.6717(6)°, γ = 82.5520(9)°, V = 2911.11(10) Å^3, Z = 2; D_{calc} = 1.643 g/cm^3. N = 10 202 unique reflections were measured using ω scans for 4.08 < θ < 25.05. The structure was solved by direct methods and refined on F^2 for all reflections with $I > 2\sigma(I)$ using 799 parameters and full-matrix least squares in SHELXTL97[15] to yield the structure with R_1 = 0.0793 and wR_2 = 0.1932; for all data, R_1 = 0.1111 and wR_2 = 0.2140. See Table 1 for parameters at lower temperatures, for which R_1 and wR_2 improve. The crystal and structural parameters in CIF format were deposited at the Cambridge Crystallographic Databank Center, CCDC No. 272168.

3-[3-(*N*-*tert*-Butyl-*N*-(*tert*-butyldimethylsiloxyl)amino)phenyl]-pyridine. A flask charged with 0.279 g (1.77 mmol) of 3-bromopyridine and 0.021 g (0.092 mmol) of palladium(II) acetate was evacuated and backfilled with argon three times. Dry tetrahydrofuran (10 mL) was added, and the suspension allowed to stir for 10 min. Deaerated solutions of 0.742 g (2.29 mmol) of boronic acid **5** in THF (5 mL) and 0.609 g (4.41 mmol) of potassium carbonate in distilled water (4.5 mL) were added via cannula. The stirred reaction was heated to reflux for 24 h under argon and then allowed to cool. The organic layer was separated. The aqueous layer was extracted with diethyl ether. The combined organic portions were dried over magnesium sulfate and evaporated under reduced pressure. Purification of the residue by column chromatography (silica gel, 8:2 hexanes−ethyl acetate) yielded 0.28 g (42%) of product as a clear colorless oil, which was used as is in the next synthetic step. Anal. Calcd for $C_{21}H_{32}ON_2Si$: C, 70.73; H, 9.05; N, 7.86. Found: C, 70.97; H, 9.24; N, 7.64. ^{1}H NMR (400 MHz, $CDCl_3$): δ −0.09 (broad s, 6 H), 0.93 (s, 9 H), 1.13 (s, 9 H), 7.30−7.36 (overlap m plus broad s, 4 H), 7.50 (broad s, 1 H), 7.83−7.86 (ddd, 1 H, J = 7.83, 2.28, 1.52 Hz), 8.57−8.58 (dd, 1 H, J = 4.80, 1.77 Hz), 8.83−8.84 (dd, 1 H, J = 2.28, 0.76 Hz).

3-[3-(*N*-*tert*-Butyl-*N*-hydroxylamino)phenyl]pyridine. Concentrated HCl (1 mL) was added to a solution of 0.10 g (0.28 mmol) of 3-[3-(*N*-*tert*-butyl-*N*-(*tert*-butyldimethylsiloxyl)amino)phenyl]-pyridine in ethanol (5 mL). The solution was allowed to stir under argon overnight, concentrated under vacuum, and then diluted with distilled water (5 mL). The resulting solution was adjusted to pH 5 with 1 M sodium hydroxide and extracted with dichloromethane. The combined organic portions were dried over magnesium sulfate and evaporated under reduced pressure to yield 0.04 g (61%) of pale yellow crystalline powder, mp 144−147 °C. Anal. Calcd for $C_{15}H_{18}ON_2$: C, 74.35; H, 7.49; N, 11.56. Found: C, 74.18; H, 7.30;

(15) Sheldrick, G. M. *SHELXTL97 Program for the Refinement of Crystal Structures*; University of Göttingen: Göttingen, Germany, 1997.

N, 11.58. ^{1}H NMR (400 MHz, $CDCl_3$): δ 1.18 (s, 9 H), 7.25−7.30 (m, 4 H), 7.43 (s, 1 H), 7.79 (d, 1 H, J = 7.6 Hz), 8.56 (d, 1 H, J = 3.2 Hz), 8.78 (s, 1 H). IR (KBr disk, cm^{-1}): 3250 (broad, OH str).

3-[3-(*N*-*tert*-Butyl-*N*-aminoxyl)phenyl]pyridine (3NITPhPyr). 3-[3-(*N*-*tert*-Butyl-*N*-hydroxylamino)phenyl]pyridine (0.032 g, 0.13 mmol) was dissolved in 3.0 mL of dichloromethane under argon. Freshly prepared silver oxide was added and the suspension stirred for 1 h. Thin-layer chromatography in ethyl acetate showed appearance of a radical as an orange spot in the same location as the starting material. The suspension was centrifuged and the bright red radical solution decanted and filtered through a cotton plug. This was used directly for spectroscopic studies and as a reactant in subsequent reactions. The radical is not stable to prolonged storage and so is best used as soon as possible after preparation. ESR (benzene, room temperature, 9.645 GHz): a_N = 12.31 G; a_H = 2.00, 1.89, 1.82, 0.83 G; correlation 0.997 for fitting with Duling's WINSIM program.[16]

$Cu_2(hfac)_4(3NITPhPyr)_2$ (8). The radical solution from above was placed in a clean vial and layered with 0.066 g (0.13 mmol) of $Cu(hfac)_2$ dissolved in 0.5 mL of diethyl ether and 3.0 mL of dichloromethane. This solution was layered with 6 mL of hexanes. Dark green block crystals formed after 1 week, sinters at 66−68 °C and chars and melts 109−110 °C. Anal. Calcd for $C_{50}H_{38}O_{10}N_4F_{24}Cu_2$: C, 41.66; H, 2.66; N, 3.88. Found: C, 41.53; H, 2.72; N, 3.62. Crystallographic analysis was carried out on a Bruker P4 at ambient temperature with Mo Kα radiation: λ = 0.7107 Å, μ(Mo Kα) = 0.864 mm^{-1}; yellow plate crystals 1.00 × 0.75 × 0.10 mm; formula $C_{50}H_{38}Cu_2F_{24}N_4O_{10}$ (fw 1438); triclinic space group $P\bar{1}$, with a = 10.35900(10) Å, b = 10.40400(1) Å, c = 14.8870(2) Å, α = 91.8560(10)°, β = 94.6500(1)°, γ = 113.86500(10)°, V = 1458.73(3) Å^3, Z = 2; D_{calc} = 1.637 g/cm^3. N = 6940 unique reflections were measured using ω scans for 4.1 < θ < 27.9. The structure was solved by direct methods and refined on F^2 for all reflections with $I > 2\sigma(I)$ using 594 parameters and full matrix least squares in SHELXTL97[15] to yield the structure with R_1 = 0.0326 and wR_2 = 0.0831; for all data, R_1 = 0.0425 and wR_2 = 0.0874. The crystal and structural parameters in CIF format were deposited at the Cambridge Crystallographic Databank Center, CCDC No. 272171.

Acknowledgment. This work was supported by the U.S. National Science Foundation (NSF Grants CHE-0109094 and CHE-0415716) and the Brazilian agencies CNPq and Fundação de Amparoa Pesquisado Estado de São Paulo (Grant 99/10359-7). Support for the UMass−Amherst X-ray Structural Characterization Facility (NSF Grant CHE-9974648) and Nanomagnetics Characterization Facility (NSF Grant CTS-0116498) was also provided by the U.S. National Science Foundation. Crystallographic analyses were provided by Dr. A. Chandrasekaran and Dr. P. Khalifah. We also thank the reviewers of this paper for numerous helpful, improving recommendations.

Supporting Information Available: Crystallographic data for **1**−**3**, **7**, and **8** (including CIF format files), computational modeling of hfc data for 3NITPhPyrim, and an ESR spectrum and hfc assignments for 3NITPhPyrim. This material is available free of charge via the Internet at http://pubs.acs.org. The CIF files have been also submitted to the Cambridge Crystallographic Data Centre.

IC050435T

(16) Duling, D. R. *J. Magn. Reson.* **1994**, *B104*, 105−110.